Materials and Design 111 (2016) 60–69

Contents lists available at ScienceDirect

Materials and Design

journal homepage: www.elsevier.com/locate/matdes

Efficient additive manufacturing production of oxide- and nitride-dispersion-strengthened materials through atmospheric reactions in liquid metal deposition

H. Springer [a,*], C. Baron [a], A. Szczepaniak [a], E.A. Jägle [a], M.B. Wilms [b], A. Weisheit [b], D. Raabe [a]

[a] Max-Planck-Institut für Eisenforschung GmbH, 40237 Düsseldorf, Germany
[b] Fraunhofer Institut für Lasertechnik, 52074 Aachen, Germany

HIGHLIGHTS

- Atmospheric reactions during liquid metal deposition for oxide and nitride particles
- Control of type, size and dispersion through deposition parameters, base materials and partial pressures
- Proof of principle resulted in formation of Cr2N and MnCrO in stainless steel
- Novel route for ODS and NDS materials without powder metallurgy processing

GRAPHICAL ABSTRACT

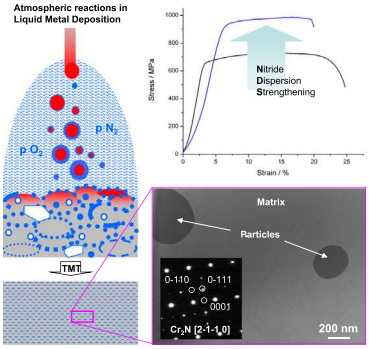

ARTICLE INFO

Article history:
Received 28 June 2016
Received in revised form 25 August 2016
Accepted 29 August 2016
Available online 30 August 2016

Keywords:
ODS steel
Dispersion strengthening
Additive manufacturing

ABSTRACT

Despite being extremely attractive compounds for strengthening, oxides and nitride particles have found only limited use in metallic materials design, as obtaining appropriate size and dispersion up to now necessitates production by time- and cost-intensive powder metallurgy processes. Here we present an alternative production method, based on the oxide and nitride formation during liquid-metal-deposition procedures in oxygen and/or nitrogen containing atmospheres. Rapid solidification of the small liquid zone suppresses floatation and agglomeration of particles, while subsequent thermo-mechanical treatments densify the material and aids particle dispersion. The in-situ particle formation coupled to the high deposition rates ensures a drastically shortened production chain. The feasibility of the method is exemplarily demonstrated on austenitic stainless steel and commercially available deposition techniques as used in additive manufacturing, performed without shielding gas but instead at air. Even without substantial optimisation of processes and material, >2 vol.% of hard and stable Cr_2N particles with sizes down to 80 nm could be evenly dispersed, resulting in pronounced strengthening at both room temperature and 700 °C without significant loss in ductility. Future possibilities for creating novel generations of cost effective and lean high strength materials, especially for high temperature applications, are outlined and discussed.

* Corresponding author.
E-mail address: h.springer@mpie.de (H. Springer).

http://dx.doi.org/10.1016/j.matdes.2016.08.084
0264-1275/

1. Introduction

The strength of metallic materials can be raised by the implementation of defects into their crystal lattice, such as solute foreign atoms, dislocations, grain boundaries or twins, all aimed at impeding the movement of dislocations as the carriers of plastic deformation. Hard and strong particles in sub-micrometric size are commonly used for precipitation strengthening (i.e. acting as obstacles for dislocations), and to increase the number of grain boundaries (i.e. refining the grain size; Hall-Petch effect) through enhanced recrystallization during thermo-mechanical treatments (TMT) [1]. In steels, as the most common high performance structural materials, the former process is for example exploited in maraging [2], tool [3] and tempered martensitic steels [4], whereas the latter is used for example in grain-refined construction [5] and high strength interstitial free steels [6]. Typical particles employed for this purpose range from alloy carbides to intermetallic phases and finely dispersed metallic copper clusters [7]. All these phases are typically precipitated from homogeneous supersaturated matrices such as austenite or martensite in steel by quenching the material from temperatures at which they are thermodynamically instable to a lower temperature where the precipitate phase becomes stable. This has the advantage that the precipitate size and especially dispersion can be easily controlled in the solid state by appropriate TMT parameters. However, their limited stability or even instability at elevated temperatures means in turn that they can undergo substantial growth or even get dissolved at high service temperatures, and thus lose their strengthening effect [1,7]. This is especially relevant for high temperature applications such as energy conversion or reactor vessels, as these phenomena limit the lifetime of parts and/or their maximum operational temperature, and thus the efficiency of the desired processes [8]. Furthermore, as many of these particles consist of comparatively rare and strategically important alloying elements, such as molybdenum (Mo), titanium (Ti) or niobium (Nb), they represent an important cost factor despite their rather small concentration in the bulk material.

In view of these requirements for the design of such particle strengthened alloys; not only for steels but also for aluminium (Al) and Ti based materials, oxides and nitrides have been identified as extremely promising candidates for corresponding blends. They mostly consist of cheap and readily available elements (e.g. Al_2O_3) and, more importantly, due to their ionic/covalent bonding, are of high strength and stable up to and beyond the liquidus temperature even of iron (Fe) based metallic matrices (i.e. steels). Furthermore, oxides and nitrides are less susceptible to radiation interaction phenomena such as swelling damage occurring in fusion and fission reactors [9]. This is exploited in oxide-dispersion-strengthened (ODS) steels, where through the introduction of about 0.5 wt.% yttria particles into stainless steel matrices, superior creep strength at elevated temperatures can be reached [10]. A particle size of a 50 nm and less has been found to be ideal, as thus a balance between cutting (if particles are too small) and circumvention (if too large) of moving dislocations is struck, thus optimising their strengthening effect [1].

Despite these great advantages over for example conventional tempered martensitic steels, though, ODS steels are the only commercially fabricated materials relying on strengthening through oxides or nitrides, and they have not found use yet in high temperature applications other than fusion reactors [11]. This is due to the substantial efforts associated with the production of such materials, particularly related to ensuring homogeneous size and dispersion of the particles in the matrix: Oxides and nitrides are not only already formed as stable compounds in the liquid phase, but also strongly deviate in density (ρ) from metals (e.g. ρ of Al_2O_3 3.95 g cm^{-3}, vs. Fe 7.85 g $cm^{-3}$and Al 2.71 g cm^{-3}, respectively [12]). Thus, whether they are injected ex-situ or formed in-situ within the melt, they rapidly float to the top (i.e. form a slag) or sink to the bottom of the melt. Even though this macroscopic segregation can be reduced by stirring procedures, which become more difficult to employ with increasing melt temperatures (e.g. from Al alloys to steel), it is extremely difficult to control the particle's meso- and microscopic dispersion, as even the smallest pre-prepared particles tend to form clusters during solidification of the cast ingot [13,14,15]. As the mechanical properties of the bulk material strongly depends on the particle size and dispersion, these phenomena make cost efficient liquid metallurgy production with established casting procedures, such as block and strip-casting, not feasible. As a consequence such materials have to be produced by powder metallurgy routes, which can ensure optimum size and dispersion of oxide and nitride particles, but at the price of numerous and complex processing steps as sketched on the left hand side in Fig. 1a. It thus becomes clear that it is of high interest to develop a synthesis route for oxide/nitride strengthened materials which combines the efficiency of liquid metallurgy production with the highly controlled particle dispersion of powder metallurgy.

2. Objective

In order to allow for a more effective production of dispersion strengthened metallic materials, we propose to utilise the formation of oxides and nitrides during liquid metal deposition. Respective techniques range from thin coating processes (e.g. arc, plasma and oxy-fuel spraying; deposited thicknesses < 1 mm), to deposition-welding (e.g. by Arc, Laser and electronic beam processes; deposited thicknesses < 10 mm), and bulk compaction techniques (such as spray-compaction; deposited thickness > 10 mm) [16]. Recently, liquid metal deposition techniques have received considerably more interest and corresponding refinement of the associated processes for additive manufacturing (AM; mainly performed by Laser-powder methods [17]). In all these techniques, the presence of the oxygen (O) and nitrogen (N), induced either by the base materials or mainly atmospheric contamination, is unwanted, as the typically associated deterioration of the mechanical properties is unfavourable for the objective of near-net-shape manufacturing of parts or coatings [18,19].

As sketched in Fig. 1b, atmospheric reactions during liquid metal deposition lead to several types of phenomena, here listed on the example of O present in the atmosphere of the deposition process: (i) The metal to be deposited is liquefied by the heat source provided by the process and is then dispersed into droplets (e.g. by electromagnetic forces in arc-processes), whose surfaces oxidise during flight to the base material. While very small particles may transform entirely into metal oxide, the oxide shells of larger ones are broken up as the (liquid or still hot and soft) particle hits the surface and solidifies there. (ii) Due to strongly reduced solubility of O in solid metal compared to liquid, micro-pores are formed during solidification of the droplets (or the melt pool if present, as for example in transferred arc processes) whose inner surface is coated by thin oxide films. (iii) Larger pores are formed when the chosen processing parameters lead to overlapped deposition of droplets, trapping atmospheric gas. The extent and kinetics of all these phenomena strongly depend on the chosen process parameters, such as chemical composition of the deposited material, partial pressures of the constituents of the atmosphere, as well as temperature, flight time and velocity of the liquid metal droplets. However, as the liquid zone of liquid metal deposition processes is much smaller than for bulk casting procedures (fractions of mm up to tenths of mm compared to several cm or even meters), the solidification proceeds much quicker and thus no pronounced floatation of oxides can be observed. In some liquid metal deposition processes, convection in the melt pool may be substantial, helping further to keep the oxides evenly distributed in the melt. These ´trapped` oxides together with the porosity are the reasons for the deteriorated mechanical performance of as-deposited materials, and thus, in the case of welding, subject of extensive efforts to minimise them.

However, subsequently applied TMTs (such as hot rolling) can effectively break up the oxide scales, disperse them in the matrix and close pores, as it is well known from hot rolling of non-killed steel [7].

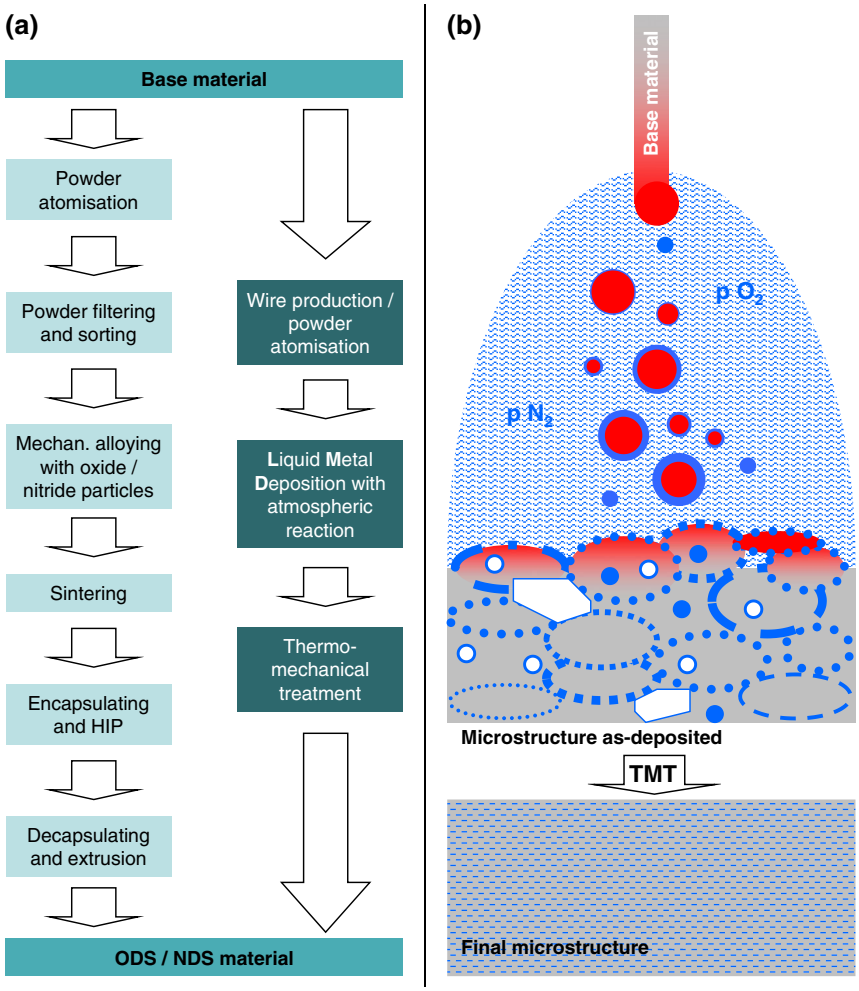

Fig. 1. (a) Process chains for the production of oxide/nitride dispersion strengthened (ODS/NDS) materials following the established methodology (left) and the approach developed in this work (right). (b) Schematic sketch of the in-situ particle formation during liquid metal deposition under oxygen and nitrogen containing atmospheres.

Furthermore, the oxides and also the nitrides may form in a metastable crystal structure upon deposition and transformation to the most stable structure at elevated temperatures (during TMT and/or annealing). We thus propose to utilise liquid metal deposition processes with controlled atmospheric reactions as a basic synthesis step for oxide or nitride strengthened metallic materials. The drastically shortened chain of production (Fig. 1a, right hand side) renders the proposed route as extremely promising to open novel pathways for the alloy design of innovative materials. In this work we exemplify achievable microstructures and properties of this novel synthesis route on stainless steel and arc/Laser deposition processes, and outline possible future routes for process and material development.

3. Materials and methods

3.1. Synthesis and processing

The feasibility of the proposed approach is exemplarily demonstrated on a commercially available stainless steel containing about 18.5 chromium (Cr), 11 nickel (Ni), 2.5 molybdenum (Mo) and <0.02 carbon (C; all in wt.%). Two liquid metal deposition techniques were deployed, the chemical composition of the respective base materials are listed in Table 1: (i) Using a 0.8 mm thick wire (Böhler EAS-4-MIG; 1.4430; SG X2CrNiMo 19 12; no fluxes) a block of about 40 mm width, 80 mm length and 20 mm thickness was produced by manual deposition welding (5 layers of about 4 weld beads beside each other) with an arc-welding machine (Lincoln Electric SP 250-I) on a 10 mm thick stainless steel base plate. Deposition was performed using standard welding parameters (wire speed 9 m min^{-1}; 20 V; welding speed about 5 mm s^{-1}), but at air without any shielding gas. We refer to these materials throughout the manuscript as "Arc" samples. (ii) Atomised stainless steel 316 L powder (1.4401; X5CrNiMo17 12 2 2; powder size of 30–70 μm) was deposited by nozzle-based Laser Metal Deposition (LMD; Laser power 930 W, speed 10 mm s^{-1}, offset between deposition passes 875 and 250 μm in y and z direction, respectively) to a block of about 30 mm width, 100 mm length and 15 mm thickness on a stainless steel base plate of about 5 mm thickness. The powder was transported into the interaction zone of laser beam and substrate using argon (Ar) as carrier gas (gas flow 3 L min^{-1}). However, the additional argon gas flow inside the powder feed nozzle was shut off which reduces the shielding of the melt pool significantly. We refer to these

Table 1
Chemical composition of all materials throughout the different processing steps in wt.%, obtained by wet chemical (Fe as balance).

	Cr	Ni	Mo	Mn	Si	C	O	N
Wire (for Arc)	18.3	11.7	2.57	1.21	0.74	0.010	0.007	0.044
Powder (for Laser)	17.7	10.8	2.41	1.18	0.53	0.0196	0.064	0.073
Arc (as-deposited)	19.1	12.4	2.62	0.93	0.51	0.012	0.01–0.14	0.62
Laser (as-deposited)	18.4	10.7	2.41	0.90	0.34	0.025	0.25–0.46	0.077
Casting (as-cast)	18.2	11.4	2.58	1.21	0.65	0.005	0.020	0.003
Arc (as-rolled)	17.6	11.8	2.54	1.01	0.59	0.009	0.21–0.47	0.56
Laser (as-rolled)	18.5	10.8	2.40	0.88	0.37	0.019	0.68–0.83	0.079
Casting (as-rolled)	18.3	11.6	2.62	11.18	0.67	0.005	0.06	0.004

materials throughout the manuscript as "Laser" samples. Additionally, a reference material of similar chemical composition as the to be deposited base materials was produced by vacuum induction melting of a 1 kg charge, and casting into a copper (Cu) mould of 20 × 20 mm^2 internal cross section. No particle dispersion strengthening is expected in this material. We refer to these materials throughout the manuscript as "Casting" samples. After deposition, the base plates were sawn off, and all three materials (Arc, Laser, Casting) were hot rolled under air at 1100 °C to a final thickness of 2 mm and cooled at air to room temperature.

It should be highlighted that neither the base material represents the optimum for ODS materials, nor were the deposition techniques optimised for the synthesis of particle reinforced materials. We chose them to prove the feasibility of the approach with readily available materials and techniques, and outline future optimisation steps based on the derived results.

3.2. Characterisation and testing

Microstructures were investigated on cross sections and longitudinal sections, ground and polished with standard metallographic techniques by optical microscopy (OM; Zeiss Axiophot 1) and scanning electron microscopy (SEM; Jeol JSM6500F) equipped with electron backscatter diffraction analysis (EBSD; TSL system with OIM software). Samples for analysis by transmission electron microscopy (TEM; Jeol-2200FS were prepared by a liftout technique in a focused ion beam system (FIB; FEI Helios Nanolab 600i). Particles were quantified on SEM images (magnification 2000) by image analysis using the ImageJ software package. Mechanical properties were probed by tensile testing of flat dog-bone shaped samples parallel to the rolling direction on samples with a gauge length of 10 mm and a width of 3 mm, at an initial strain rate of 10^{-3} s^{-1}. Tensile testing was performed both at room temperature and at 700 °C (both at air). Chemical composition of all materials throughout the processing steps was determined by wet chemical analysis.

4. Results

4.1. Microstructure evolution

Microstructures of all three materials directly after synthesis are shown in Fig. 2. Within the as-deposited Arc material (Fig. 2a), OM images (left) reveal several large pores filled with slag (several 100 μm in diameter), stemming from irregular overlapping of the weld beads due to the manual deposition. Otherwise the material is free of defects (i.e. no cracks), but a high density of evenly dispersed small dark features can be observed in the SEM images at higher magnification (middle). Typical for as-welded microstructures, the austenitic grains are elongated due to the direction of heat flux towards the base plate, and have an average size of about 110 μm according to EBSD analysis (right). The as-deposited microstructure of the Laser material (Fig. 2b) is similar, only the number of larger pores is decreased due to the automated deposition procedure. Again a large number of evenly dispersed small dark features can be observed within the microstructure. The grains are more equiaxed and with about 7 μm in diameter much smaller than those of the Arc material, however, due to the more rapid solidification of the much smaller melt pool. The Casting material (Fig. 2c) is largely free of pores and particles, but, as it can be expected from the much slower solidification of the comparatively large ingot, the grains size is at >300 μm much larger than those from both Arc and Laser materials and indications of interdendritic segregation can be observed.

Compared to the respective base materials (i.e. wire and powder), the deposition processes left the C levels virtually unchanged, but raised the O concentration by about one order of magnitude (Table 1), i.e. to 0.01–0.14 wt.% for the Arc material and up to 0.25–0.46 wt.% for the Laser material. The higher O concentration in the Laser material is not

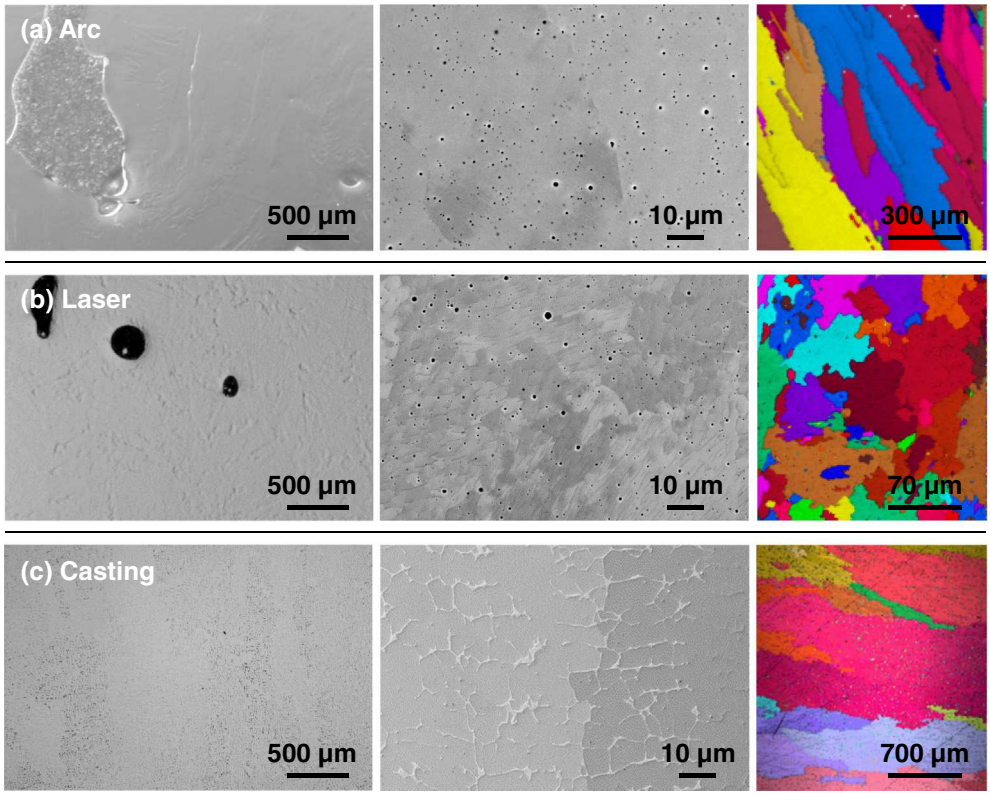

Fig. 2. Overview of the microstructures directly after synthesis. Left: OM images showing occasionally occurring large slag inclusions due to the non-optimised deposition techniques. Middle: SEM images showing evidence of particle inclusions and interdendritic segregations. Right: EBSD maps colour-coded for grainsize.

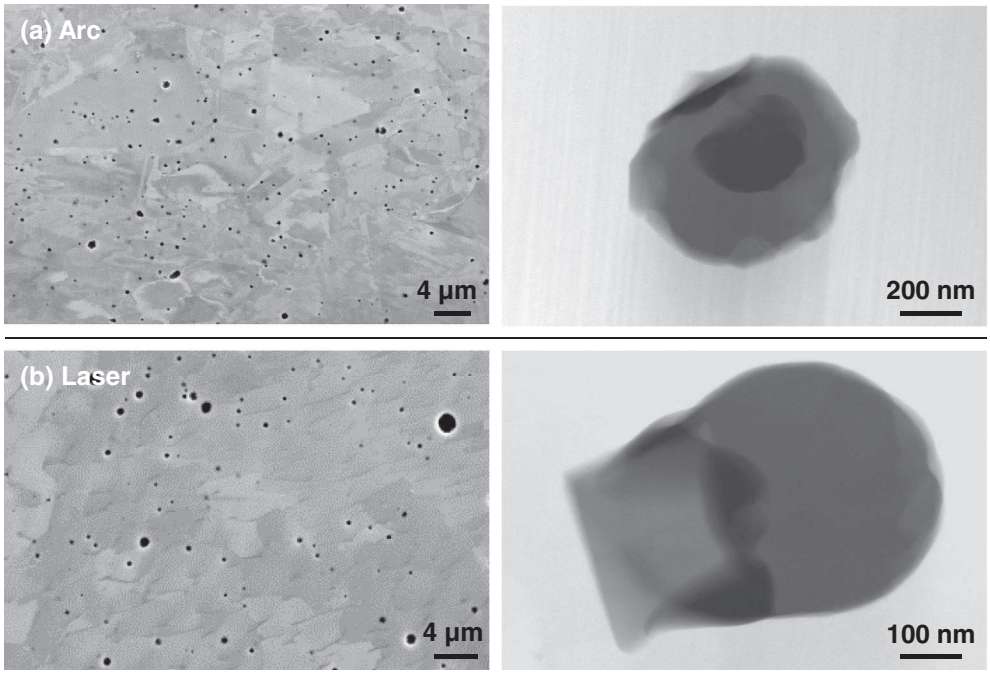

Fig. 3. Higher resolution images for the materials directly after synthesis by SEM (left) and TEM (STEM HAADF; right). (a) Si-rich oxides and Cr-rich nitrides in the Arc material. (b) Complex oxides in the Laser material.

only related to the process characteristics, but also to the larger surface area of the powder, thus carrying more O with it than the wire (0.064 compared to 0.007 wt.%, respectively). As the large scatter of the O concentrations indicates, though, it cannot be excluded that the obtained values were affected by slag particles, e.g. by a large pore present in the probed volume for chemical analysis. Interestingly, the N concentration in the Arc material shows a strong increase to 0.62 wt.%, whereas it remains almost unchanged in the Laser material. The content of the other alloying elements Cr, Ni and Mo stays constant or slightly increases with both deposition techniques, meaning that Fe as balance was preferably evaporated, and the levels of Mn and Si dropped by about a third. The O concentration of the Casting material is slightly higher and the N concentration lower than of the base materials used for deposition by Arc and Laser.

SEM images of higher magnification (left in Fig. 3) revealed the small features present in as-deposited materials to be sub-micron sized pores and particles. Most of the features on the polished cross sections appear to be re pores, but a major fraction of them most probably stem from particles being partly or fully removed from the matrix during sample preparation (mechanical polishing). The sample preparation by FIB for TEM analysis, on the other hand, did not lead to removal of particles. As can be expected for the as-deposited microstructures, which are far from thermodynamic equilibrium, the formed particles are distributed inhomogeneously both in size and type. As shown in the images on the right hand side of Fig. 3, the particles within Laser and Arc material are complex O-rich structures consisting of several chemically different compounds (Si-O, Mn-Si-O, Mn-Cr-O) as determined by EDS analysis in TEM. Only $MnCr_2O_4$ could be identified by diffraction analysis in the TEM. It should be stressed that sample preparation of such particle reinforced materials as well as comprehensive particle identification is complex, and O (and N) quantification need increased effort for example by atom probe tomography [20]. As the statistics of such high resolution characterisation are limited, the presence of additional phases - such as nitrides in the Arc material - cannot be excluded. Within the Casting material, no particles could be found, except for very few Mn-oxides, and ceramic residues stemming from the crucible material.

Quantification results of the sizes of particles within the as-deposited Arc and Laser material are compiled in Fig. 4. The particles in the Arc material (Fig. 4a) have an average diameter of 0.41 µm (minimum 0.18, maximum 1.16 µm without the large slag-filled pores), a number density of 0.051 μm^{-2} and a volume fraction of 0.805%. Within the Laser

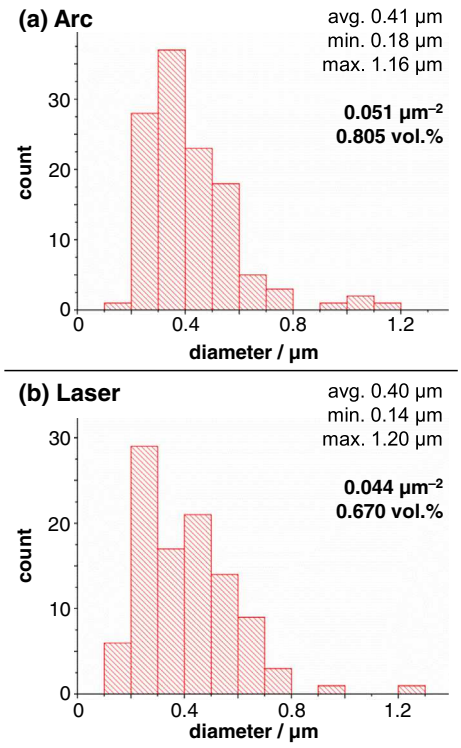

Fig. 4. Quantification results of the particles within Laser and Arc material directly after synthesis.

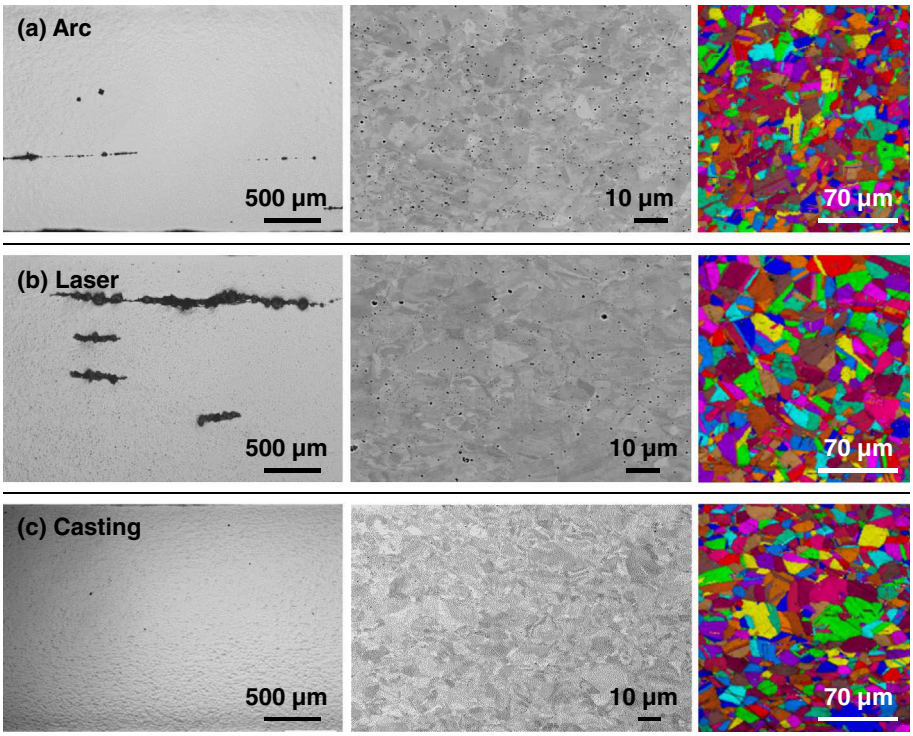

Fig. 5. Overview of the microstructures after hot rolling. Left: OM images showing elongated slag lines stemming from the non-optimised deposition techniques. Middle: SEM images. Right: EBSD maps colour-coded for grainsize.

material (Fig. 4b) the particles are of very similar size, but of a reduced number density (0.044 μm^{-2}) and lower volume fraction (0.670%).

Hot rolling changes the initial as-synthesised microstructure severely (Fig. 5). All three materials recrystallised to a similar austenitic matrix grain size of 12.5 µm (Arc), 6.7 µm (Laser) and 10.6 µm (Casting). The large slag-filled pores in the Arc and Laser material, as artefacts from the non-optimised deposition techniques (a subject of future investigations), were compressed and elongated to slag-lines about 50 µm thick and up to a few millimetres in length. The corresponding chemical composition (Table 1) stayed virtually unaffected compared to the as-deposited state, except for the O concentration, which was roughly doubled to 0.21–0.47 wt.% for the Arc material and 0.68 – to 0.83 wt.% for the Laser material. Characterisation results of the as-rolled microstructures with higher magnification (Fig. 6) revealed an

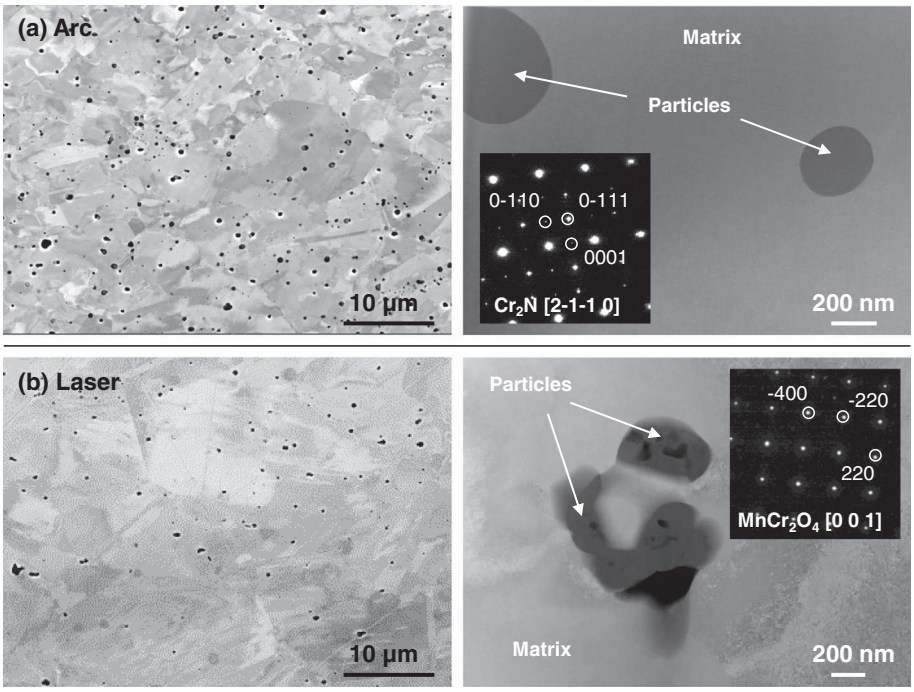

Fig. 6. Higher resolution images for the materials hot rolling by SEM (left) and TEM (STEM HAADF; right). (a) Cr_2N identified in the Arc material. (b) $MnCr_2O_4$ identified in the Laser material.

increased number of evenly dispersed particles, which could be identified by TEM exclusively as nitrides (type Cr_2N) within the Arc material (Fig. 6a), and oxides (type $MnCr_2O_4$) in the Laser material (Fig. 6b). According to the standardless quantitative EDS analysis the composition of Cr_2N (Fig. 6a) was determined as (79-82)Cr–6N–(7-11)Fe–2V–2Mo–1Mn, whereas $MnCr_2O_4$ (Fig. 6b) was of the composition 49O–33Cr–17Mn–1Al (all in at.%). Again, these results should be seen in light of the well know difficulties of quantifying the concentration of the light elements N and O by EDS. The thermo-mechanical treatment not only changes the type, but also refines the particle size from the as-deposited state and increases the number density (Fig. 7). The particles in the Arc material exhibit a larger scatter in diameter. The increased O concentrations (Table 1) correspond to strongly increased fractions of 0.960 vol.% in the Laser material, and 2.241 vol.% in the Arc material, which contains less O but more N. Again, inadvertent inclusion of slag-lines into the chemical analysis cannot be ruled out.

4.2. Mechanical properties

Tensile testing results of all three materials after hot rolling are shown as representative engineering stress/strain curves in Fig. 8. At room temperature (Fig. 8a) the casting material (black solid curve) shows a yield stress (YS) of about 500 MPa, slight work hardening to an ultimate tensile stress (UTS) of about 700 MPa and a total elongation (TE) of close to 25%. The Laser material (blue curve) exhibits a slightly lower YS and UTS (600 and 650 MPa, respectively), and an enlarged TE of about 35%. The Arc material, on the other hand, shows a pronounced strengthening (red curve), raising YS to about 950 MPa, UTS close to 1000 MPa and only slightly reducing TE to about 20%. While a similar strength level could be reached by cold rolling (50% reduction in thickness) the reference Casting material, this leads to significant embrittlement.

As shown in Fig. 8b, all materials lose significant strength at 700 °C. The TE values remains roughly similar to the room temperature testing results, but the uniform elongation is significantly lowered and almost

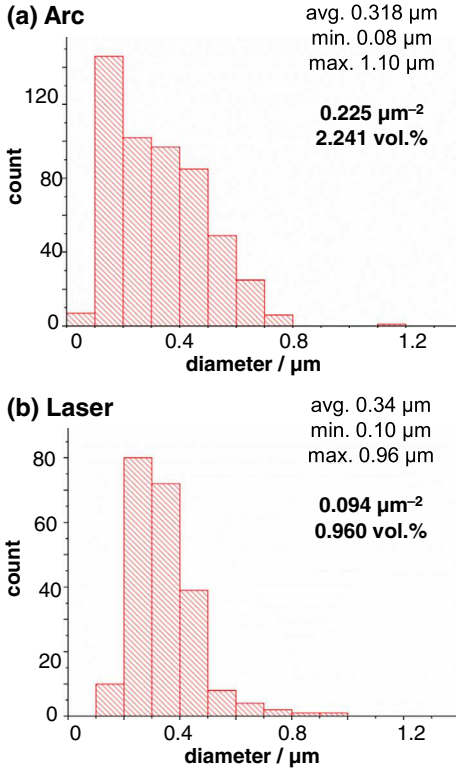

Fig. 7. Quantification results of the particles within Laser and Arc material after hot rolling.

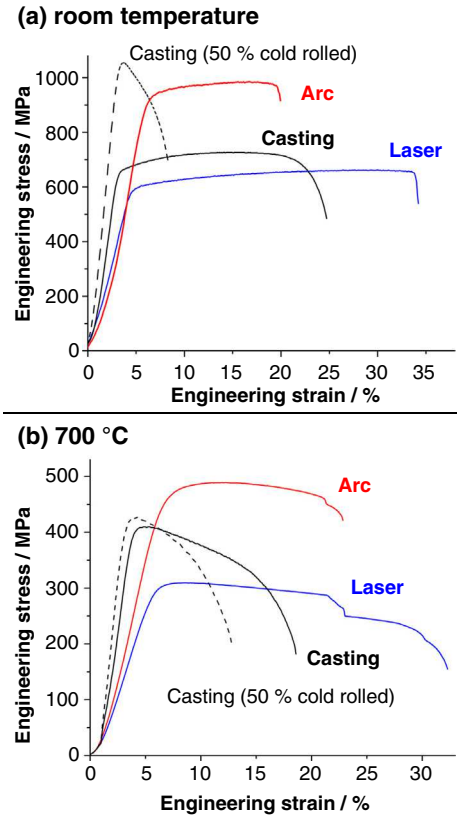

Fig. 8. Tensile testing results of all materials at room temperature (a) and 700 °C (b).

no work hardening can be observed. Both Laser (blue) and Casting (solid black) materials exhibit a similar drop of about 300 MPa from their room temperature UTS. The strengthening of the Casting material induced through cold rolling is fully eliminated (dashed curve), bringing it down to the same level as the hot-rolled material. The Arc material, on the other hand, retains a UTS of almost 500 MPa and TE of about 20% at this elevated temperature.

The deviating elastic regimes of the tensile curves are artefacts from different setting behaviour of the materials in the formfitting clamps of the testing machine. The occasionally found slag lines within both Arc and Laser materials were formed parallel to the tensile direction, and only in the samples used for testing at elevated temperature evidence of their influence on the mechanical behaviour could be observed, and then only in the post-necking regime.

5. Discussion

5.1. Evolution of microstructure and mechanical properties of the model alloys

Our results clearly demonstrate how atmospheric reactions in liquid metal deposition can be utilised to effectively synthesise bulk metallic materials reinforced with oxide and/or nitride particles of submicrometric size and optimum dispersion. Even with a very basic setup such as Arc welding of a conventional stainless steel at air followed by hot rolling, more than to 2 vol.% of Cr_2N nitride particles with submicrometric size could be evenly dispersed in an austenitic matrix.

As the as-deposited state with its short flight time of liquid droplets and rapid solidification is far away from thermodynamic equilibrium, rather complex oxides of the most reactive elements Mn and Si are formed (Fig. 3) instead of the more stable phases such as Cr_2O_3 [21]. Interestingly, the Arc material not only shows a lower O uptake than the Laser material, but also contains an order of magnitude higher amount

of N (Table 1), and consequently nitrides additional to oxide particles can be observed. Apparently, either the Ar used in the Laser synthesis as a carrier gas for the stainless steel powder lowered the N_2 partial pressure of the atmosphere relative to the O_2 partial pressure, or the plasma of the Arc process contained dissociation of N_2 and thus to diffusible N. Even though the standard Gibbs free energies of formation for many oxides are much lower than those for nitrides (e.g. ΔG^0_f at 1100 K: Cr_2O_3–565 kJ mol^{-1} vs. Cr_2N − 75 kJ mol^{-1} [21]), the higher partial pressure of nitrogen in air in the arc process favours nitriding reactions and the higher O_2 partial pressure in the partially-inert atmosphere in the laser process favours oxidising reactions. Subsequent hot rolling, however, leaves the material for a longer time at elevated temperature allowing for the formation of more stable particles, i.e. dominantly Cr_2N within the Arc material and $MnCr_2O_4$ within the Laser material (Fig. 6). It is well known that already the addition of a few tenths of percent of Mn to chromia-forming steels leads to the formation of the spinel phase $(Mn,Cr)_3O_4$ upon oxidation due to the high rate of diffusion of Mn atoms as compared to Cr atoms [22,23,24]. This is for example commonly observed during the service life of stainless steel interconnects in solid oxide fuel cells [25,26], and the formation of $MnCr_2O_4$ in our experiments is therefore not unusual. Further transformations of particle phases could possibly be achieved by longer annealing times, but the thermodynamics and kinetics of reactions within the bulk material (and not for the better understood surface reactions), with the additional factor of deformation energy induced by the thermo-mechanical processing, are difficult to predict. While the N level stays roughly constant, the O content of both materials is about doubled through the hot rolling, most probably via oxidation of open channels in the initially porous bulk sheets. More importantly, though, the size of particles is decreased and their number density increased (Figs. 4 and 7) due to conversion of gas trapped in pores into oxide particles, as well as breaking-up and dispersion of already formed particles (if they have suitable morphology such as shells around initial pores). As more nitrides are found in the Arc material after hot rolling compared to the as-deposited state despite similar N content, it appears that nitrides additionally precipitate from a supersaturated solid solution and not formed exclusively during the flight time of liquid droplets during synthesis. The solubility of O and especially N in the solid state strongly depends on the material system, in our case increased by the high Cr content of the chosen stainless steel [7].

The achieved fine dispersion of particles is the main factor explaining the drastically differing mechanical performance compared to the reference casting material, as they exhibit a similar grain size of the austenitic matrix (Fig. 5). While the lower volume fraction of oxide particles within the Laser material leads to a slight softening and ductilisation, the Arc material with its higher concentration of nitride particles shows a high strength level without sacrificing ductility (Fig. 8). Apart from the higher volume fraction, this can be attributed to increased hardness of the nitride particles (hardness of Cr_2N about 26 GPa) and/or differences in residual stresses around the particles (from different thermal expansion coefficients of particles and matrix) and interfacial energies. Detailed investigations concerning the precise nature of particle/matrix interaction during deformation, however, are exceeding the focus of this paper which is concerned with a proof-of-principle of the synthesis approach. Nonetheless, the strengthening achieved by the nitrides is not only more effective than that achievable by plastic deformation such as cold rolling, but is also retained to elevated temperatures (i.e. that is still stronger than the reference material at identical temperature), as the small and hard nitride particles appear to strongly decrease the mobility of dislocations and internal interfaces. Most probably this strengthening – which allows referring to such materials as nitride-dispersion-strengthened (NDS) steels – also translates into improved creep life compared to established tempered martensitic steels, due to the higher thermodynamic stability of nitrides compared to alloy carbides. The mechanical performance of our trial material is not yet on the same level as well-developed and established high temperature materials such as ODS steels produced by powder metallurgy [9,27,28], but the already satisfactory results highlight the yet untapped potential of our approach for future alloy design.

5.2. Consequences for alloy and process design

This work is focused on proving the feasibility of our approach to effectively synthesise ODS and NDS materials. While only basic material and techniques were used, the obtained results allow for identifying critical parameters for the targeted development and optimisation of synthesis technology and respective alloy compositions. In this manner not only established ODS alloy concepts can be synthesised more effectively, but it allows to open novel pathways for the design of structural materials.

The type of particles can be effectively controlled by the chemical composition of the base materials, i.e. the wire or powder used in the liquid metal deposition process. For example Si or Ti can be added to form respective nitrides, while e.g. Y or Al can be used to promote the formation of alumina or yttria. As the desired strengthening and/or grain refinement is achieved by the oxide and/or nitride particles, the amount of costly and critical elements such as Nb, Ta or V required for alloy carbides in high strength steels, can be reduced. Another example for future alloy design possibilities is the development of steels for high temperature applications. Here the Cr content can be increased above the maximum level of tempered martensitic steels (about 12 wt.%) in order to achieve improved corrosion resistance, as no austenitisation for martensitic transformation and carbide precipitation is required. However, the proposed approach is not limited to steels, but can also be readily transferred to effectively synthesise particle-reinforced nonferrous systems such as Al, Ti or even Mg alloys for high performance lightweight materials.

Another factor controlling the type of atmospheric reaction and especially their respective kinetics are the respective partial pressures. From a practical perspective, this is most easily achievable by controlled O_2 and/or N_2 additions to inert gases such as Ar. Especially O_2 appears to be critical, as it leads to violent exothermic reactions, and thus to unwanted burn-off of elements and slags, which is most relevant for highly reactive Al, Mg or Ti systems. If high C steel matrices are targeted, pronounced loss of C via CO/CO_2 formation could be compensated for by hydrogen additions. As the particles produced in this study are small enough to show a pronounced strengthening effect, they are on average still large compared to those in ODS steels produced by mechanical alloying (Fig. 7). Their size and also dispersion, however, can be modified via the respective parameters of the chosen liquid metal deposition technique: In Arc-processes for example, it is well known that the voltage/current settings can be utilised to achieve different characteristic types of metal transfer, and thus influence size, flight time and temperature of the liquid metal droplets [16]. Other important factors are the interlayer-temperature between the LMD passes (affecting the cooling rate), as well as the geometrical build-up and chosen TMT settings (for example deposited beads of changing direction, coupled to hot rolling transverse to the plane of deposition).

The feasibility of bulk liquid metal deposition for the cost effective production of large and highly loaded machine components has already been successfully demonstrated, for example on cups for high performance water turbines produced by Arc-welding of super-martensitic steel [29]. A respective setup adapted for the production of ODS and NDS materials is sketched in Fig. 9. In view of the key requirements of low equipment costs, high deposition rate and readily controllable atmospheric conditions and metal transfer, Arc-welding and spray-compaction processes appear most promising for a production chain as sketched in Fig. 1a. Powder processes such as Laser-based setups used in additive manufacturing typically offer higher geometrical control and the possibility to manufacture near-net shaped parts of precise dimensions, but are generally slower and more expensive.

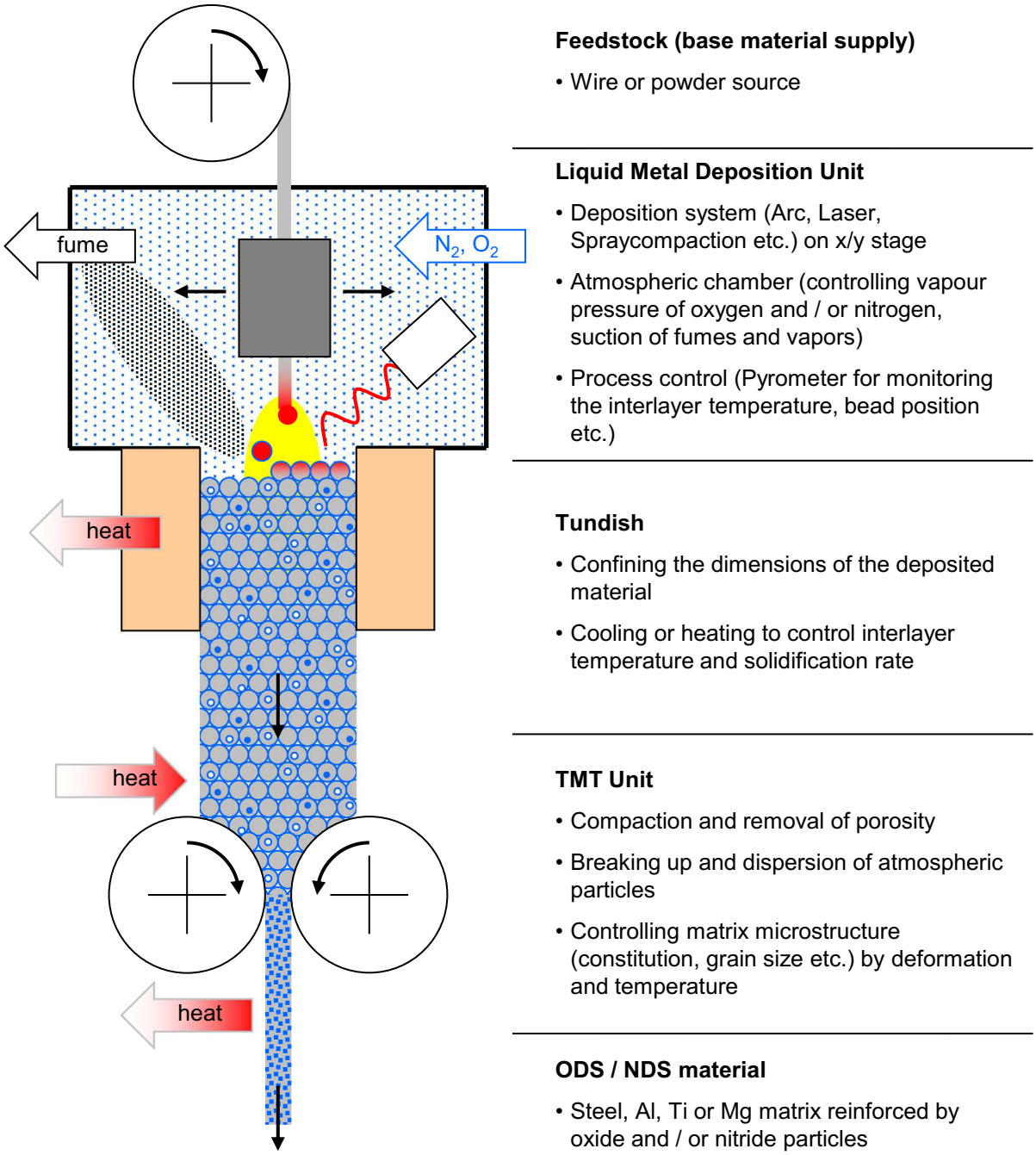

Fig. 9. Schematic sketch of upscaling the synthesis procedure for ODS/NDS material on an industrial scale.

6. Summary and conclusions

We have demonstrated how large quantities of metallic materials reinforced by strong and thermodynamically stable particles can be effectively synthesised by liquid metallurgy techniques. The approach is based on utilising atmospheric reactions in liquid metal deposition, where oxide and nitride particles are formed during synthesis under an oxygen and/or nitrogen containing atmosphere. The rapid solidification of the small liquid zone effectively suppresses floatation and clustering of particles, while subsequent thermo-mechanical treatments break them up, further disperse them and remove porosity. The result is an efficient and dramatically shortened production chain compared to established powder metallurgy-based procedures. The approach is demonstrated with two commercially available deposition techniques, namely Arc-welding and Laser-powder deposition, performed without shielding gas but at air, using a conventional stainless steel as a base material. The following conclusions can be drawn:

(1) In the as-deposited state, both Laser and Arc materials show a strong increase in O content and contained finely dispersed oxide particles of complex build-up. Within the Arc material, and additionally strong increase of the N concentration up to 0.62 wt.% and formation of Cr-nitrides was found.
(2) Hot rolling at 1100 °C at air decreased the average particle size from to about 400 μm to 300 μm, and increased their volume fraction and number density. The Arc material contained

>2 vol.% and 0.23 μm^{-2} Cr_2N particles, whereas the within the Laser material $MnCr_2O_4$ particles of roughly half the volume fraction and number density were observed.

(3) While the Laser material showed slightly less strength and increased ductility compared to the cast-and hot-rolled reference material, the Arc material showed a strong increase in strength without significant embrittlement. This particle-induced benefit in strength was retained at 700 °C, whereas strengthening via cold deformation of particle-free material did not only lead to pronounced loss in ductility at room temperature, but also was fully alleviated at elevated temperature.

(4) Neither the deposition techniques nor the base materials were optimised for the chosen synthesis approach. Strong improvements in particle size and dispersion, as well as to avoid unwanted formation of slags, could be achieved by adjusting the deposition parameters of the chosen deposition technique, such as the voltage/current setting in Arc welding. Key parameters to obtain desired types of particles are the base material composition (with designated alloying additions for oxide or nitride phases) and partial pressure of the gases in the deposition atmosphere.

(5) The developed approach allows for opening novel pathways in the design of structural materials, especially for high temperature applications. ODS alloys can be synthesised more efficiently, bringing them out of their specialised niche and the amounts of costly alloying elements in high strength steel concepts can be reduced. The synthesis procedure is also transferable to other metallic matrices such as Al and Ti, allowing for the volume production of new generations of high performance lightweight materials.

Acknowledgements

H. Springer wishes to thank M. Rohwerder for valuable discussions concerning the kinetics and thermodynamics of the atmospheric reactions. Financial support from the Accelerated Metallurgy Project, which is co-funded by the European Commission in the 7th Framework Program (contract NMP4-LA-2011-263206), is gratefully acknowledged.

References

[1] M.F. Ashby, Materials Selection in Mechanical Design, Butterworth-Heinemann, Burlington, MA, 2005.
[2] J. Millána, S. Sandlöbes, A. Al-Zubib, T. Hickel, P. Choi, J. Neugebauer, D. Ponge, D. Raabe, Acta Mater. 76 (2014) 94–105.
[3] T. Večko Pirtovšek, G. Kugler, M. Terčelj, Mater. Charact. 83 (2013) 97–108.
[4] F. Abe, Precipitate design for creep strengthening of 9% Cr tempered martensitic steel for ultra-supercritical power plants, Sci. Technol. Adv. Mater. 9 (2008) 13002.
[5] D. Belato Rosado, W. De Waele, D. Vanderschueren, S. Hertelé, Sustainable construction and design5th International Conference on Sustainable Construction and Design, 2013.
[6] R. Rana, W. Bleck, S.B. Singh, O.N. Mohanty, Development of high strength interstitial free steel by copper precipitation hardening, Mater. Lett. 61 (2007) 2919–2922.
[7] H. Berns, W. Theisen, Eisenwerkstoffe Stahl und Gusseisen, Springer Verlag, Berlin, Heidelberg, 2006.
[8] O. Prat, J. Garcia, D. Rojas, G. Sauthoff, G. Inden, Intermetallics 32 (2013) 362–372.
[9] Z. Oksiuta, P. Olier, Y. de Carlan, N. Baluc, Development and characterisation of a new ODS ferritic steel for fusion reactor application, J. Nucl. Mater. 393 (2009) 114–119.
[10] J. Chao, C. Capdevila, Anisotropy in mechanical properties and fracture behavior of an oxide dispersion Fe20Cr5Al alloy, Metall. Mater. Trans. A 45 (3) (2014) 767.
[11] S.J. Zinkle, G.S. Was, Materials challenges in nuclear energy, Acta Mater. 61 (2013) 735–758.
[12] M.F. Ashby, Materials Selection in Mechanical Design, Butterworth-Heinemann, Burlington, MA, USA, 2005.
[13] S.C. Tjong, Z.Y. Ma, Mater. Sci. Eng. R 29 (2000) 49.
[14] J.W. Kaczmara, K. Pietrzak, W. Wøosin Âski, The production and application of metal matrix composite materials, J. Mater. Process. Technol. 106 (2000) 58–67.
[15] Y. Feng, Strengthening of steels by ceramic phasesPhD thesis RWTH Aachen, 2013.
[16] S. Kou, Welding Metallurgy, second edition John Wiley & Sons, Inc., Hoboken, New Jersey, USA, 2003.
[17] I. Gibson, D. Rosen, B. Stucker, Additive manufacturing technologies, 3D printing, rapid prototyping, and direct digital manufacturing, second edition Springer, New York Heidelberg Dordrecht London, 2010.
[18] E.O. Olakanmia, Selective laser sintering/melting (SLS/SLM) of pure Al, Al–Mg, and Al–Si powders: effect of processing conditions and powder properties, J. Mater. Process. Technol. 213 (2013) 1387–1405.
[19] L. Loh, C. Chua, W. Yeong, J. Song, M. Mapar, S. Sing, Z. Liu, D. Zhang, Numerical investigation and an effective modelling on the selective laser melting (SLM) process with aluminium alloy 606, Int. J. Heat Mass Transf. 80 (2015) 288–300.
[20] A. Hirata, T. Fujita, Y.R. Wen, J.H. Schneibel, C.T. Liu, M.W. Chen, Atomic structure of nanoclusters in oxide-dispersion-strengthened steels, Nat. Mater. 10 (2011) 922.
[21] T.B. Reed, Free Energy of Formation of Binary Compounds, MIT Press, Cambridge, MA, 1971.
[22] H.J. Yearian, E.C. Randell, T.A. Longo, Corrosion 12 (1956) 515–525.
[23] F.H. Stott, F.I. Wei, C.A. Enahoro, Mater. Corros. 40 (1989) 198–205.
[24] A.L. Marasco, D.J. Young, Oxid. Met. 36 (1991) 157–174.
[25] J.W. Fergus, Mater. Sci. Eng. A 397 (2005) 271–283.
[26] J.E. Hammer, S.J. Laney, R.W. Jackson, K. Coyne, F.S. Pettit, G.H. Meier, Oxid. Met. 67 (2007) 1–38.
[27] S. Ukai, M. Harada, H. Okada, M. Inoue, S. Nomura, S. Shikakura, T. Nishida, M. Fujiwara, K. Asabe, Tube manufacturing and mechanical properties of oxide dispersion strengthened ferritic steel, J. Nucl. Mater. 204 (1993) 74–80.
[28] M.A. Sokolov, D.T. Hoelzer, R.E. Stoller, D.A. McClintock, Fracture toughness and tensile properties of nano-structured ferritic steel 12YWT, J. Nucl. Mater. 367–370 (2007) 213–216.
[29] Patent by Andritz Hydro AG, Obernauerstrasse 4, 6010 Kriens, Switzerland